Deposition Patterns of Aerosolized Drugs Within Human Lungs: Effects of Ventilatory Parameters

Ted B. Martonen[1,2,4] and Ira M. Katz[3]

Received September 8, 1992; accepted December 27, 1992

A mathematical model for inhaled aerosolized drugs is validated by comparisons of predicted particle deposition values with experimental data from adult subject inhalation exposure tests. The model is subsequently used to study the effects of ventilatory parameters on particle deposition patterns within the human lung. By altering breathing profiles, deposition values can be affected regarding quantity delivered and spatial location. Increased tidal volumes and breath-holding times increase deposition in the pulmonary region, while increased inspiratory flow rates increase deposition in the tracheobronchial region. Based upon fluid dynamics considerations (Reynolds numbers), an original method of partitioning the lung is also presented. The model has implications with regard to aerosol therapy, indicating that the efficacies of inhaled pharmacological drugs in the prophylaxis and treatment of airway diseases can be improved by regulating breathing profiles to deposit particles selectively at prescribed sites within the lung.

KEY WORDS: inhaled drugs; particle deposition; mathematical model.

INTRODUCTION

The administrations of pharmacologic drugs via inhalation have two fundamentally different applications: (a) lung dosimetry and, (b) systemic delivery. An important conclusion of clinical research pertinent to aerosol therapy protocols is that drug efficacy and patient response are related to particle deposition patterns among lung airways (1–18).

The issue of lung dosimetry relates to the efficacies of inhaled medicines in the treatment of airway diseases. The lung per se is the target organ and the site specificities of deposited drugs may be the key factors involved in eliciting therapeutic effects. Let us now consider some clinical cases and pharmacologic drugs from the medical literature (cited above) where site specificities have been described in terms suggesting focal (e.g., "bifurcations") to regional (e.g., "central airways") dimensions. Some data indicate that certain bronchodilator drugs should be selectively delivered to well-defined, small areas such as tracheobronchial bifurcations, perhaps preferentially at carinal ridges (16). Likewise, the prophylaxis of chronic obstructive lung diseases would improve from the preferential deposition of airborne pharmaceuticals among more distal airways. Examples of broader site-specific therapeutic effects are patient responses to anticholinergic agents targeted to the larger central airways of the lung, whereas β-adrenergic agonists affect the smaller central and peripheral airways (2,3). Although the precise morphological position of a drug deposition–patient response interaction may not be unambiguously determined, or may be known only in regional terms, the mechanism involved can often be relatively well defined. For instance, it is thought that disodium cromoglycate, commonly prescribed in the treatment of bronchial asthma, acts specifically on the surface of mast cells blocking the release of inflammatory mediators (17).

The clinical observations cited above may be explained at least partially in terms of the spatial distributions of appropriate receptors and nerve endings among lung airways. The respective distributions could range in character from being heterogeneous (e.g., localized) to homogeneous (e.g., uniform). Consider the first case. Karlsson *et al.* (8) studied the variant roles of afferent neural pathways and determined, as an example, that upper tracheobronchial (TB) branching sites (i.e., bifurcations) are especially sensitive to stimulation of cough. They suggested that rapidly adapting stretch receptors (RARs) may function as "cough receptors" commensurate with the relatively high concentrations of RARs in the proximal airways of the tracheobronchial tree and the superficial locations of RARs within the mucosa. This would be consistent with the observed fast blocking effect of topically applied or aerosolized anaesthetics. Let us now address the second case. Barnes *et al.* (4), using autoradiography techniques, reported the first mapping of the distributions of β-receptors within the lung. They detected a dense labeling of smooth muscle that was greater in small (i.e., bronchioles) than large (i.e., cartilaginous bronchi) airways. The potent bronchodilator effect of β-agonists, therefore, may be due to the rather widespread (albeit not uniformly so) dispersion of β-receptors throughout the lung.

Regarding (b), i.e., systemic delivery, the lung may be the chosen avenue of entrance into the body. Deposited drugs may then be distributed via the circulatory system. Still, particle deposition patterns may be of importance since enhancement of deposition in the alveolated airways would promote the dissemination of drugs, via the bloodstream, to desired target organs.

Let us put an aerosol therapy protocol into perspective. The nature of a particular disease will determine the inhaled drug to be prescribed for its treatment. In turn, the available aerosols will be produced using certain established techniques; metered dose inhalers (MDIs), dry powder inhalers (DPIs), and nebulizers are usual options, depending upon whether inpatient or outpatient care is in order. The subsequent deposition patterns of inhaled drugs depend upon (i) aerosol characteristics (e.g., particle size, shape, and den-

Disclaimer: Although the research described in this article has been supported by the United States Environmental Protection Agency, it has not been subjected to Agency review and therefore does not necessarily reflect the views of the Agency and no official endorsement should be inferred. Mention of trade names or commercial products does not constitute endorsement or recommendation for use.

[1] Health Effects Research Laboratory, U.S. Environmental Protection Agency, Research Triangle Park, North Carolina 27711.

[2] Division of Pulmonary Diseases, Department of Medicine, University of North Carolina, Chapel Hill, North Carolina 27514.

[3] Department of Engineering Science, Trinity University, San Antonio, Texas 58212.

[4] To whom correspondence should be addressed at Mail Drop 74, HERL, U.S. EPA, Research Triangle Park, North Carolina 27711.

0724-8741/93/0600-0871$07.00/0

sity), (ii) lung morphology, and (iii) breathing profiles. In usual clinical situations the characteristics of the aerosols, factor i, produced by MDIs, DPIs, and nebulizers, cannot be readily controlled or adjusted. Likewise, variations in lung morphology, factor ii, are representative of real intersubject differences among a population. But it may be possible to regulate the patient's ventilatory parameters, factor (iii), to permit pharmacologic drugs to be selectively deposited among lung airways so as to elicit optimum therapeutic effects. This text examines the influences of breathing profiles with a *validated* model.

The regulation of breathing affords a rare opportunity to enhance the efficacies of inhaled pharmaceuticals. Of course, it may not be a viable alternative in all clinical circumstances. For instance, the manifestation of certain respiratory disease states may preclude attempts to substantively control ventilation. Therefore, the treatment of patients with impaired pulmonary function may prove to be more difficult than, for example, the administration of prophylactic agents to asthmatics and the delivery of medicines with systemic activities to patients with normal lung functions.

In practice, it is often difficult to establish an unambiguous correlation between deposition sites and therapeutic effects of medicinal agents due to the complexities involved in clinical drug testing and evaluation regimens. To the point, it is very difficult to determine exactly where particles have been deposited in the lung. To overcome this difficulty, we suggest that mathematical modeling may be conducted in a complementary manner with laboratory administrations of inhaled drugs.

It has been suggested by Dolovich *et al.* (19) that breathing profiles (i.e., tidal volumes and respiratory frequencies) may exert a pronounced influence upon the behavior and fate of inhaled pharmaceuticals. More recently, Newman *et al.* (20) and Malmberg *et al.* (21) have performed clinical studies examining effects of inspiratory flow rates upon drug delivery and patient response. Herein, a new mathematical model is used to investigate the effects of ventilatory parameters on particle deposition within the human lung.

The model is first validated with the inhalation exposure results of Heyder *et al.* (22), which summarize the extensive and systematic series of experiments performed with human subjects under controlled conditions. Then, the model is employed with several well-defined breathing profiles to specifically identify the effects of inspiratory flow rates, tidal volumes and breath-hold times on deposition patterns.

METHODS: DEFINITION AND VALIDATION OF THE AEROSOL DEPOSITION MODEL

The system of equations developed by Martonen (23) is used to describe the deposition efficiencies of the processes of inertial impaction, sedimentation, and diffusion for inhaled particles. The equations describe the motion of an inhaled particle in terms of geometric size and material density, assuming a spherical particle shape. In the mathematical simulation of particle behavior the dispersion of an inhaled bolus of aerosol is monitored throughout the lung in the manner described by Martonen *et al.* (24). Entrained particles are continuously removed from the bolus (i.e., deposited) during a breathing cycle. To determine cumulative deposition, the influence of each mechanism is calculated independently and then combined using the statistical technique of superposition (25).

To use the aerosol deposition computer code it is necessary to select a lung morphology consisting of individual airway dimensions and network branching patterns. We shall use Weibel's Model A morphology to describe the adult human lung (26). It is a symmetric, dichotomously branching network of cylindrical tubes. Previous work has shown the system to be preferential to an asymmetric morphology for aerosol deposition modeling purposes (27). The tracheobronchial (TB) compartment consists of 17 generations of conducting airways (I) numbered from 0 (trachea) through 16 (terminal bronchioles). The pulmonary (P) compartment consists of 7 generations of alveolated airways numbered from 17 (respiratory bronchioles) through 23 (alveolar sacs). Each generation I consists of 2^I identical airways.

In Fig. 1, the four sets of stylized breathing profiles considered are illustrated. In Fig. 1A, the inspiratory flow rate (i.e., slope of the solid line) of a test subject is fixed at Q = 500 Ml/sec and the tidal volume (TV) is varied; this permits effects upon particle deposition related to the depth of aerosol penetration into the lung to be calculated. In Fig. 1B, a patient would inspire to the same TV value (i.e., 1000 mL) over different times (2, 4, and 8 sec), so the effect of Q upon particle deposition is revealed by varying it from 250 to 1000 mL/sec. In Fig. 1C, the effects of breath-hold times can be studied. In Fig. 1D, the time increments of a breath are set; for a prescribed inspiratory time (i.e., 2 sec) the TV value is varied. The combined effects of flow rate and penetration are examined with this profile, which may simulate intersubject variability among a population. For all

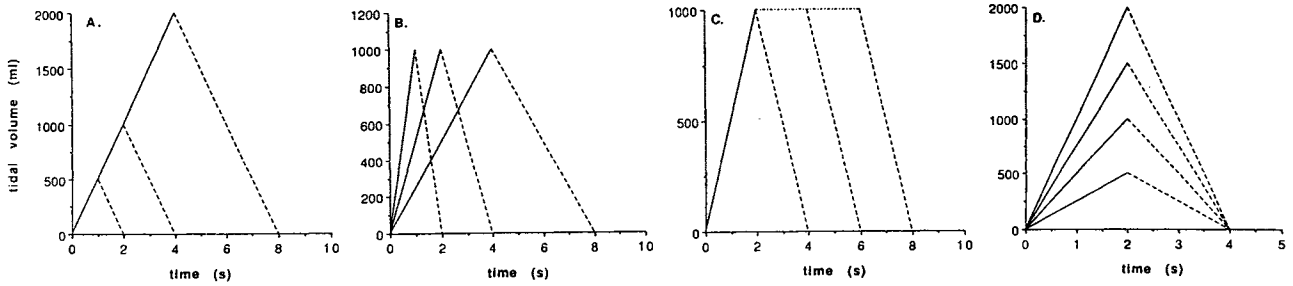

Fig. 1. Breathing profiles used to simulate a range of human conditions. (A) A constant inspiratory flow rate (Q) of 500 mL/sec with corresponding tidal volumes (TV) of 500, 1000, and 2000 mL. (B) A fixed TV of 1000 mL with Q values of 250, 500, and 1000 mL/sec. (C) TV and Q values of 1000 mL and 500 mL/sec, respectively, and breath-hold times of 0, 2, and 4 sec. (D) Changing TV and Q values: 500 and 250, 1000 and 500, 1500 and 750, and, 2000 mL and 1000 mL/sec, respectively.

of the cases described above in Figs. 1A–D, the expiratory flow rate is regarded as being equal to the inspiratory flow rate.

The particle deposition model was *validated* herein by comparisons of calculated values with the experimental data of Heyder *et al.* (22). The deposition fractions of particles are compiled for three breathing profiles used in the laboratory tests: Fig. 2, TV = 1000 mL, frequency (f) = 7.5 breaths/min, Q = 250 mL/sec; Fig. 3, TV = 500 mL, f = 15 breaths/min, Q = 125 mL/sec; and Fig. 4, TV = 1500 mL, f = 15 breaths/min, Q = 750 mL/sec.

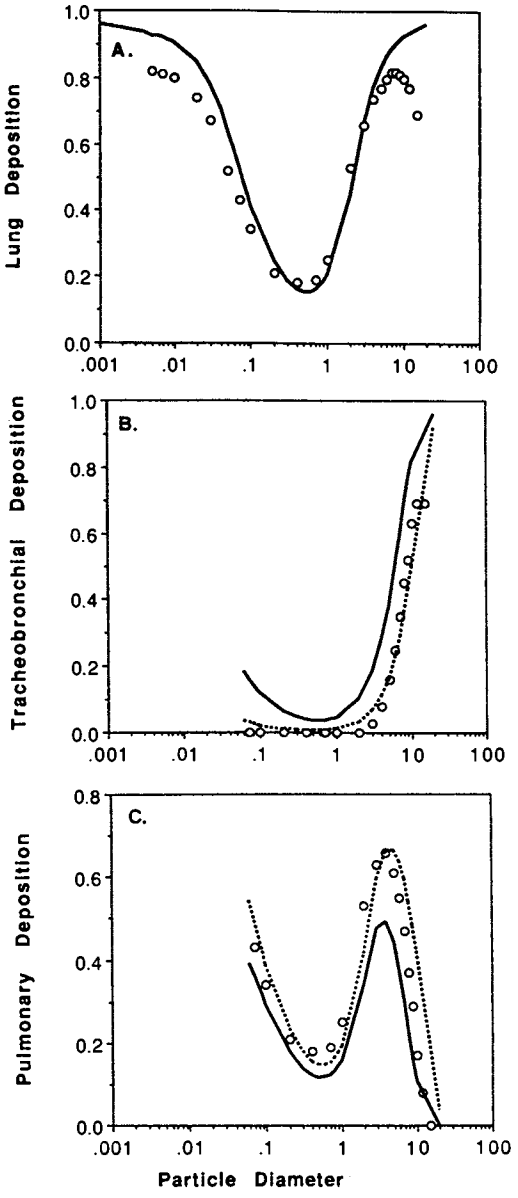

Fig. 2. Particle deposition within the whole lung (A) and its TB and P components (B and C, respectively) for the breathing pattern of TV = 1000 mL and Q = 250 mL/sec. The circles represent experimental data from Heyder *et al.* (22). In B and C the solid-line curves represent deposition in Weibel (26) generations I = 0–16 for the TB region and I = 17–23 for the P region, and the dashed-line curves indicate deposition in generations I = 0–11 and I = 12–23. Particle sizes are in micrometers.

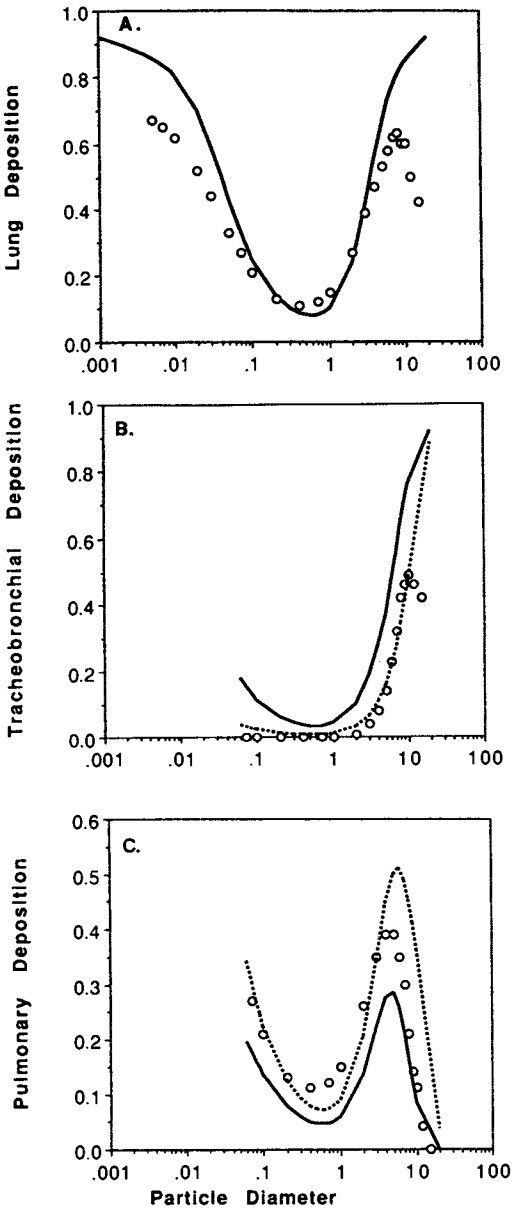

Fig. 3. Particle deposition within the whole lung (A) and its TB and P components (B and C, respectively) for the breathing pattern of TV = 500 mL and Q = 125 mL/sec. The circles represent experimental data from Heyder *et al.* (22). In B and C the solid-line curves represent deposition in Weibel (26) generations I = 0–16 for the TB region and I = 17–23 for the P region, and the dashed-line curves indicate deposition in generations I = 0–11 and I = 12–23. Particle sizes are in micrometers.

The measured total lung deposition fractions for each of these breathing profiles are shown in Figs. 2A, 3A, and 4A. There is an overall systematic pattern of deposition consisting of very high deposition fractions for particles $\leq$0.02 μm, minima for $\approx$0.5-μm particles, and deposition fractions for 5- to 10-μm particles reaching approximately the same levels as for the smallest particles. For particles in the 0.1- to 10-μm range the theoretical model not only predicts the qualitative patterns, including the relative locations of the maxima and minima, but also is in very good quantitative agreement with

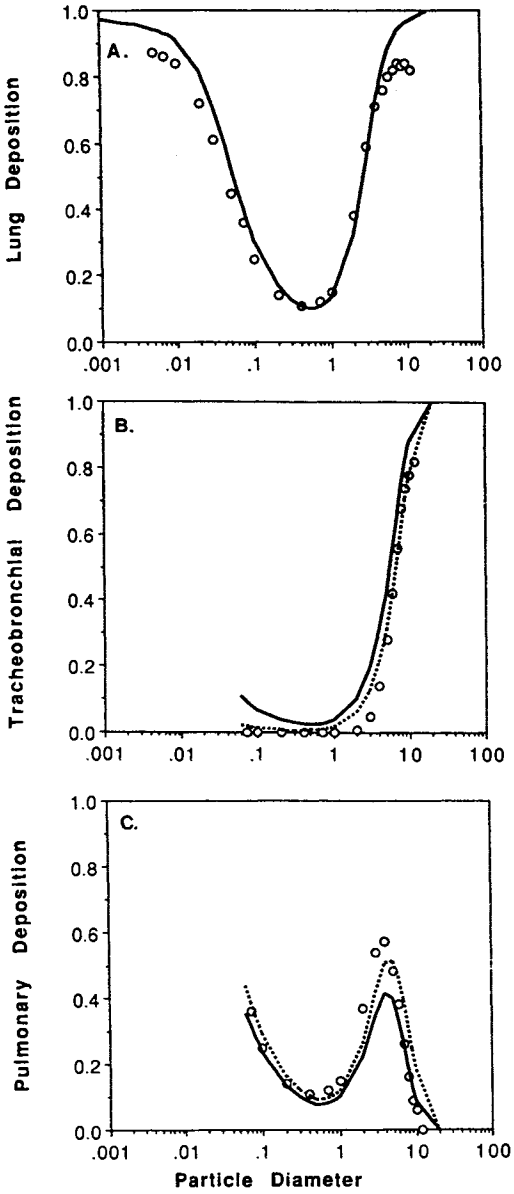

Fig. 4. Particle deposition within the whole lung (A) and its TB and P components (B and C, respectively) for the breathing pattern of TV = 1500 mL and Q = 750 mL/sec. The circles represent experimental data from Heyder *et al.* (22). In B and C the solid-line curves represent deposition in Weibel (26) generations I = 0–16 for the TB region and I = 17–23 for the P region, and the dashed-line curves indicate deposition in generations I = 0–11 and I = 12–23. Particle sizes are in micrometers.

the laboratory data. The experimental deposition fraction values decrease as particles exceed ≈10 μm, whereas model results predict an increase in deposition. This may be because the complicated fluid dynamics conditions in the upper TB compartment are not adequately accounted for in the model; specifically, we refer to effects of the laryngeal jet and associated unstable air flow patterns upon particle behavior. For particles sizes less than 0.1 μm the model tends to predict slightly higher deposition fractions than indicated by experiment. The accuracy of the model in the 0.1- to 10-μm range is of significant practical importance; particles outside of this range usually do not enter the lung, being collected in the extrathoracic region (28–31).

In Figs. 2B and C, 3B and C, and 4B and C experimental data are compared to model results for the TB and P compartments, respectively. For the ultrafine (<0.1-μm) particles, the experimental deposition fractions were not broken down compartmentally by Heyder *et al.* (22). The solid-line curves represent deposition in Weibel (26) generations I = 0–16 for the TB compartment and I = 17–23 for the P compartment. In Figs. 2B and C, 3B and C, and 4B and C the dashed-line curves represent deposition in generations I = 0–11 and I = 12–23, respectively. The reason for this distinction in lung partitioning is explained below.

Let us now address the compartmental distributions in more detail. The experimentally obtained TB deposition fractions for each breathing profile (Figs. 2B, 3B, and 4B) are zero for particles less than 1 μm. As particle sizes increase up to about 10 μm, the measured deposition values also increase. For larger particles the deposition fractions decrease, this is most clearly evident in Fig. 3B. The theoretical results are U-shaped curves without regard as to how the TB compartment is defined in terms of airway composition; that is, I = 0–16 or I = 0–11. The observed decrease in deposition for large particles is not predicted as noted above. The theoretical results begin to diverge from the data for particles less than 1 μm because they do not reflect the minimal deposition fractions of the experiments. It is apparent that the best correlation between experimental data and theoretical results occurs when the TB compartment is defined as consisting of generations I = 0–11, as opposed to I = 0–16 [i.e., the Weibel (26) definition].

The experimentally obtained P deposition fractions for each breathing profile (Figs. 2C, 3C, and 4C) have a local minimum at ≈0.5 μm and a local maximum at ≈5.0 μm. The bimodal curves of the experimental findings are accurately predicted by the theoretical model. The quantitative agreement between theory and experiment is closer when the P compartment is defined as generations I = 12–23 than I = 17–23 [i.e., the Weibel (26) definition].

Weibel (26) divided the human lung into distinct TB and P compartments based upon considerations of morphology alone. We now suggest that for particle deposition modeling purposes, the lung be partitioned into analogous regions based upon considerations of air flow characteristics. This fluid dynamics perspective is presented in Fig. 5 for a spectrum of breathing profiles defined as sedentary [TV = 500 mL, frequency (f) = 14 breaths/min, Q = 233 mL/sec], moderate (TV = 1291 mL, f = 15.5 breaths/min, Q = 667 mL/sec), and exertion (TV = 2449 mL, f = 24.5 breaths/min, Q = 2001 mL/sec). In Fig. 5A, the velocity of air within each lung generation is shown. In each case the velocity values become very small by generation I = 16. This is due to the great increase in cumulative cross-sectional area of the lung as it serially branches. The effect of this on the respective deposition mechanisms of inertial impaction, sedimentation, and diffusion can be inferred from Fig. 5B, where the fluid Reynolds number, Re, for each lung generation is shown. The fluid Reynolds number is defined as Re = UD/ν, where U denotes the average velocity, D the airway diameter, and ν the kinematic viscosity of air. The Reynolds number can be regarded as a measure of the inertia

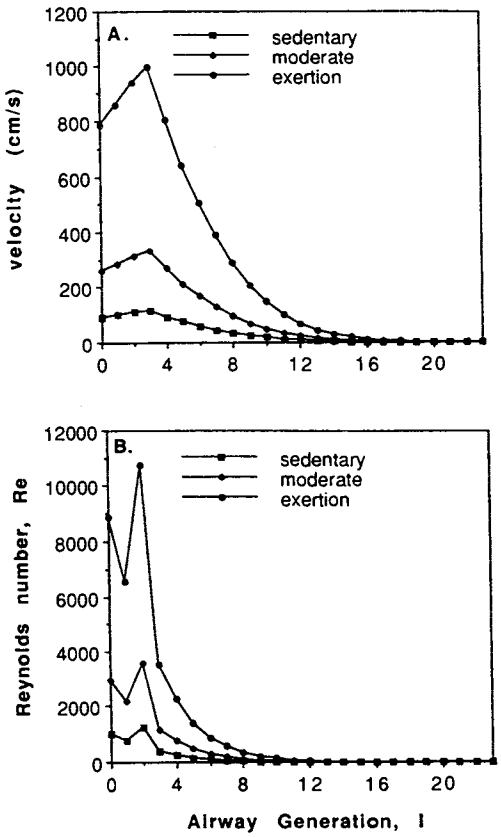

Fig. 5. The air velocity (A) and corresponding Reynolds number (Re = UD/ν) (B) for each generation of a Weibel (26) lung for sedentary, moderate, and exertion breathing conditions.

of air flow within each lung generation. For each breathing profile the fluid Reynolds number is essentially zero after generation $I = 11$. Therefore, aerosol deposition due to inertial impaction in this region (i.e., $I = 12$–23) is negligible for all of the breathing profiles considered. Deposition in this region of the lung will depend largely on the residence time of an inhaled particle, and the associated mechanisms of deposition are diffusion (i.e., random Brownian motion) for small particles and, sedimentation (i.e., settling under gravity) for large particles.

For a specific human subject, the division of experimentally derived total deposition fractions into TB and P components depends on the interpretation of gamma camera pictures and the related times assumed for the mucociliary and macrophage clearance mechanisms assigned for each region of the lung. The uncertainties involved in these measurements are well documented (32,33). In using the analytical aerosol deposition model presented herein, it must be understood that the true morphological TB and P division of a given subject may not consistently correspond to a particular generation-by-generation partitioning of the Weibel (26) definition. Likewise, the particular airway geometries of a human subject (i.e., lengths and diameters) and the model's definition may differ. By choosing the pulmonary region to consist of generations $I = 12$–23, the effects of morphological uncertainties while defining the P compartment are removed because they no longer have a relevant effect on the calculations. In practical effect, we will have succeeded in defining a region where only the diffusion and sedimentation mechanisms act efficiently; and as Heyder *et al.* (22) have explained, in the real P compartment, particle deposition will be dominated by these processes. These mechanisms depend only on the residence times of particles spent in these airways; geometric variables such as branching angles have no discernible impact on particle behavior. Throughout the balance of this paper, therefore, the TB and P compartments are defined as generations $I = 0$–11 and $I = 12$–23, respectively.

In the preceding text, predictions of the analytical model have been compared with laboratory data from human subject exposures. The agreement is excellent for particle sizes experienced in aerosol therapy protocols. There are, however, discrepancies between the theoretical results and the experimental data for ultrafine particles as well as particles greater than $\approx$10 μm in size.

RESULTS AND DISCUSSION

In Fig. 6A–C aerosol deposition patterns have been calculated for the breathing profile designated A in Fig. 1. The effects of tidal volumes on lung deposition are demonstrated in Fig. 6A. The curves are parallel (for all practical intents and purposes), with decided minima in the $\approx$0.5- to 1-μm interval. As the tidal volume varied from 500 to 2000 mL, lung deposition increased monotonically for all particle sizes, and by as much as 100% over a wide size interval (i.e., 0.03–3 μm). In Fig. 6B it is clearly demonstrated that there is virtually no change in magnitude among the U-shaped family of TB deposition curves with increasing tidal volumes at the fixed inspiratory flow rate. It can be deduced, therefore, that inspiratory flow rate is the ventilatory parameter which determines the TB deposition fraction of an inhaled aerosol. Conversely, the distinctly bimodal family of curves in Fig. 6C reveals that the increased deposition within the lung which can be ascribed to increased tidal volume breathing occurs entirely in the P region. The increased P deposition is a result of deeper particle penetration into the lung at the increased tidal volumes and the increased particle residence times in peripheral airways associated with the respective breathing profiles. The bimodal curves have peaks at about 0.02- and 5-μm sizes. For particles <0.01 and >10 μm, P deposition decreases simply because of the pronounced filtering efficiencies of the upstream TB compartment; that is, particles which could be deposited in the alveolated airways do not penetrate sufficiently into the lung.

The results for breathing profile B in Fig. 1 are presented in Fig. 7. Lung deposition (Fig. 7A) increases monotonically with the duration of a breathing cycle; that is, deposition is inversely related to inspiratory flow rate (except for sizes >10 μm). For particles <0.1 μm, the curves appear to converge to an asymptote of $\approx$0.95. TB deposition values (Fig. 7B) increase monotonically with inspiratory flow rates for large particles (>1 μm) due to increased efficiency of the inertial impaction mechanism. When particles are <0.1 μm, however, TB deposition values decrease monotonically with increases in inspiratory flow rates. For such small particles diffusion characterizes motion, thus particle residence times spent in airways are the key factors determining deposition. In this instance, the increasing inspiratory flow rate de-

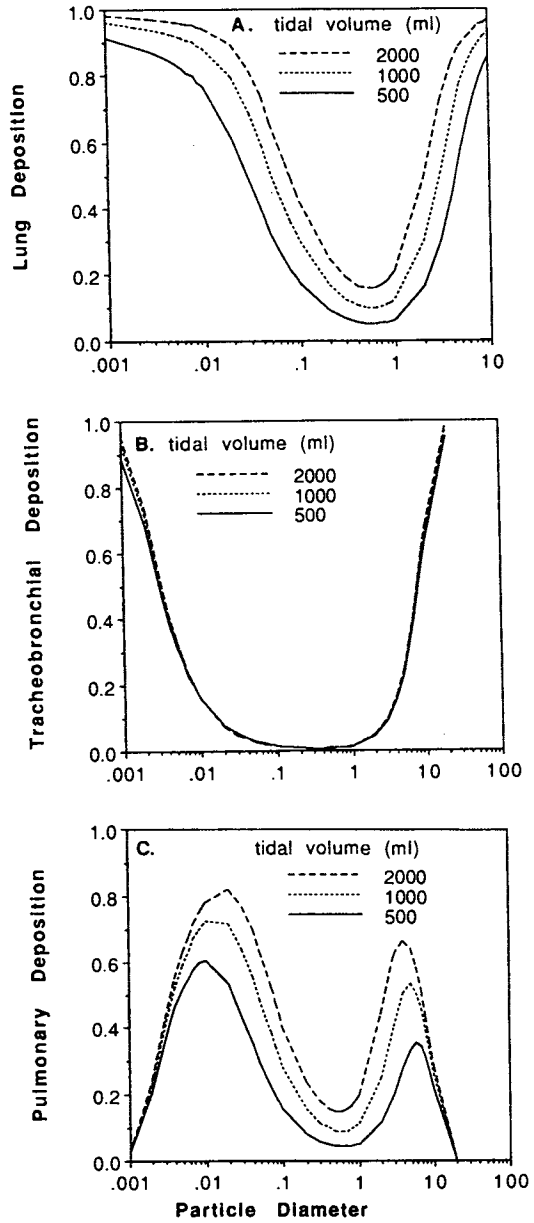

Fig. 6. Calculated particle deposition within the whole lung (A) and its TB (B) and P (C) components for breathing profile A in Fig. 1. Particle sizes are in micrometers.

creases particle residence time in the TB compartment, hence particle deposition also decreases. P deposition (Fig. 7C) is governed by particle residence times for all particle sizes, and for an increased breathing cycle (i.e., a decreased inspiratory flow rate) the mechanisms of diffusion and sedimentation have a longer time to operate, thus increasing deposition (except for particles <0.01 μm). For these smallest particles the reverse behavior is observed, namely, deposition decreases monotonically with cycle time (or increases with flow rate). This is due to the decrease in deposition within the TB compartment as flow rates increase which allows for enhanced deposition downstream. It is quite apparent that the P deposition curves reflect particle losses in the TB compartment. In total (Fig. 7A), lung deposition is more sensitive to the factor of particle residence time than inspiratory flow rate.

In Fig. 8, the results for breathing profile C in Fig. 1 are presented. The total deposition curves in Fig. 8A are essentially parallel over a wide size range (about 0.03–3 μm), then converge to asymptotes signifying a deposition fraction of 0.95 or greater for both ends of the particle spectrum. Because flow rates are unchanged in these simulations, TB deposition values (Fig. 8B) are coincident for each case examined. The effects of breath-hold times are to increase the associated residence times of particles in the lung. This produces very ordered curves in the P region (Fig. 8C) and correspondingly greater deposition with longer holding periods.

The deposition curves for breathing profile D in Fig. 1 are given in Fig. 9. The combined effect of simultaneously

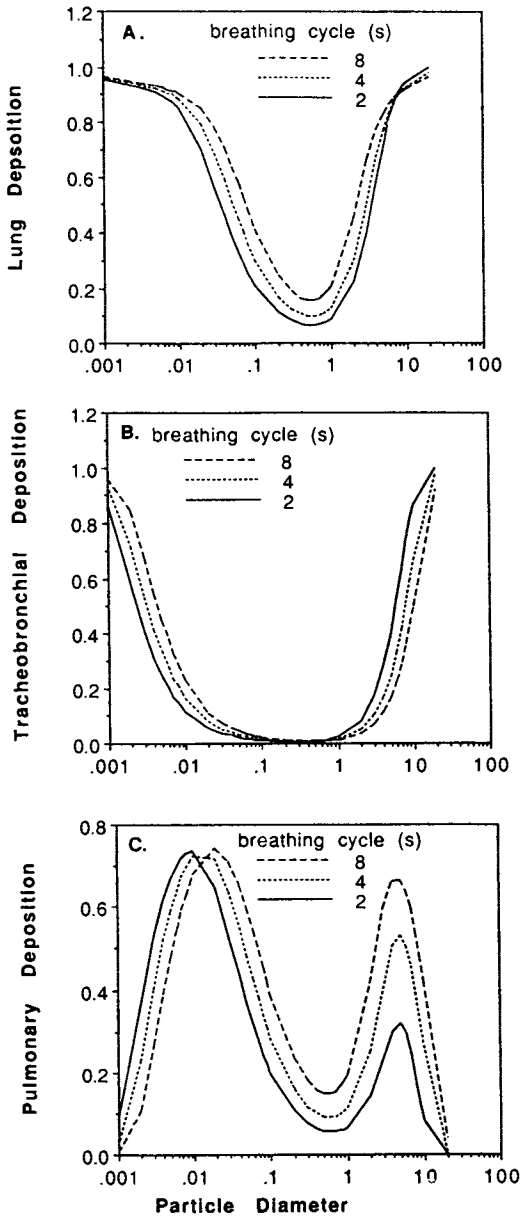

Fig. 7. Calculated particle deposition within the whole lung (A) and its TB (B) and P (C) components for breathing profile B in Fig. 1. Particle sizes are in micrometers.

increasing inspiratory flow rates and tidal volumes is to increase total deposition (Fig. 9A). The systematic family of curves has a minimum of ≈0.1 near the 0.5-μm size and increases toward 0.9–1.0 deposition for very small (<0.01-μm) and very large (>10-μm) particles. The TB deposition curves (Fig. 9B) behave as those observed for increased inspiratory flow rates alone (Fig. 7B). The P deposition values (Fig. 9C) increase monotonically with increasing tidal volumes and flow rates except for particles >3 μm, which are preferentially deposited in the proximal TB compartment. Comparable changes were witnessed in Fig. 7C.

In conclusion, analytical models can be a valuable tool in understanding factors affecting the deposition patterns of particles within the human lung. In this text a developed model has been validated by comparisons of theoretical calculations with experimental results from human subject exposures and used to study the effects of ventilatory parameters on aerosol deposition. We have demonstrated that total lung deposition and, perhaps more importantly, its spatial distribution among TB and P airways can be markedly influenced by breathing profiles. The findings have significance regarding the efficacy of aerosol therapy by indicating that inhaled pharmacologic drugs can be preferentially targeted to desired locations for the prophylaxis and treatment of airway diseases.

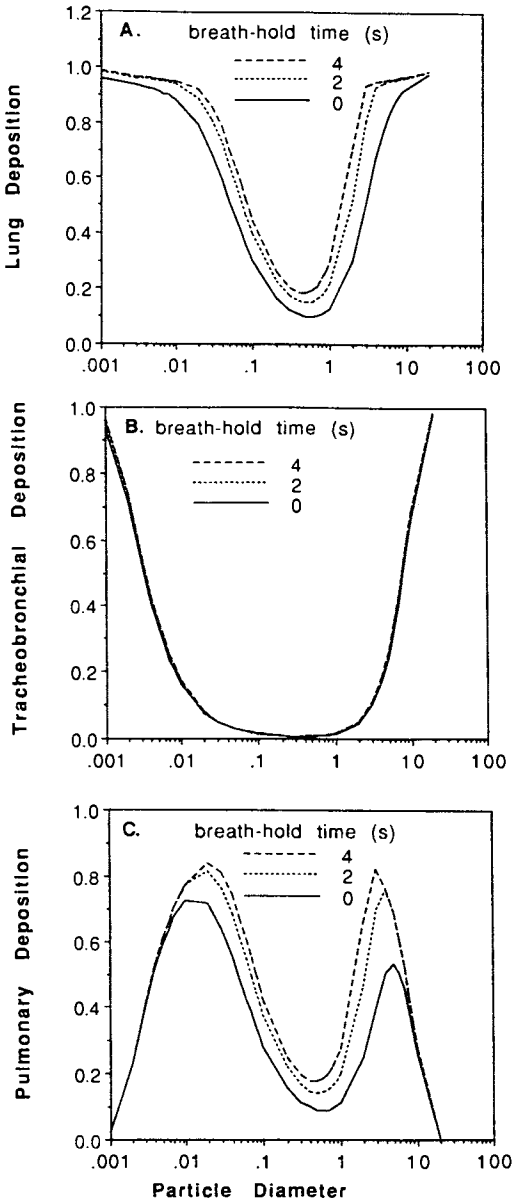

Fig. 8. Calculated particle deposition within the whole lung (A) and its TB (B) and P (C) components for breathing profile C in Fig. 1. Particle sizes are in micrometers.

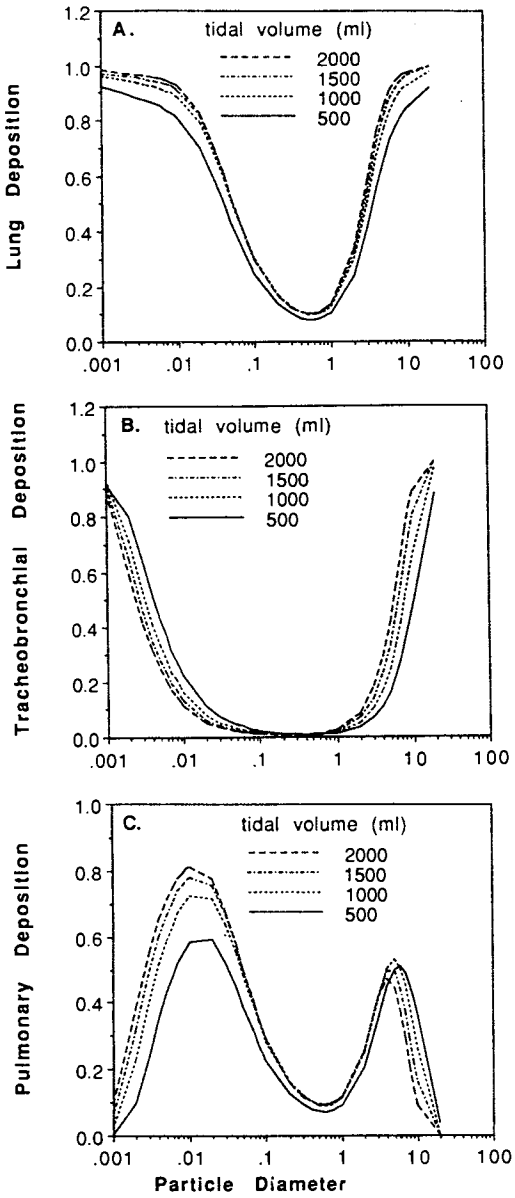

Fig. 9. Calculated particle deposition within the whole lung (A) and its TB (B) and P (C) components for breathing profile D in Fig. 1. Particle sizes are in micrometers.

REFERENCES

1. R. E. Ruffin, M. B. Dolovich, R. K. Wolff, and M. T. Newhouse. The effects of preferential deposition of histamine in the human airway. *Am. Rev. Resp. Dis.* 117:485–492 (1978).

2. M. T. Newhouse and R. E. Ruffin. Deposition and fate of inhaled aerosols. *Chest* 73S:936–942 (1978).
3. M. J. Hensley, C. F. O'Cain, E. R. McFadden, Jr., and R. H. Ingram, Jr. Distribution of bronchodilation in normal subjects, Beta agonist versus atropine. *J. Appl. Physiol.* 45:778–782 (1978).
4. P. J. Barnes, C. B. Basbaum, J. A. Nadel, and J. M. Roberts. Localization of b-adrenoreceptors in mammalian lung by light microscopic autoradiography. *Nature* 299:444–447 (1978).
5. R. E. Ruffin, M. B. Dolovich, F. A. Oldenberg, Jr., and M. T. Newhouse. The preferential deposition of inhaled isoproterenol and propranolol in asthmatic patients. *Chest* 180S:904S–906S (1981).
6. M. M. Clay, D. Pavia, and S. W. Clarke. Effect of aerosol particle size on bronchodilation with nebulized terbutaline in asthmatic subjects. *Thorax* 41:364–368 (1986).
7. D. M. Mitchell, M. A. Solomon, S. E. J. Tolfree, M. Short, and S. G. Spiro. Effect of particle size of bronchodilator aerosols on lung distribution and pulmonary function in patients with chronic asthma. *Thorax* 42:457–461 (1987).
8. J. A. Karlsson, G. Sant'Ambrogio, and J. Widdicombe. Afferent neural pathways in cough and reflex bronchoconstriction. *J. Appl. Physiol.* 65:1007–1023 (1988).
9. G. Persson and J. E. Wiren. The bronchodilator response from inhaled terbutaline is influenced by the mass of small particles, a study on a dry powder inhaler (Turbuhaler^{R}). *Eur. Resp. J.* 2:253–256 (1989).
10. G. C. Smaldone, L. Walser, R. J. Perry, J. S. Ilowite, W. D. Bennet, and M. Greco. Generation and administration of aerosols for medical and physiological research studies. *J. Aerosol Med.* 2:81–87 (1989).
11. P. J. Anderson, E. Garshick, J. D. Blanchard, H. A. Feldman, and J. D. Brain. Intersubject variability in particle deposition does not explain variability in responsiveness to methacoline. *Am. Rev. Resp. Dis.* 144:649–654 (1991).
12. H. L. Ashworth, C. G. Wilson, E. E. Sims, P. K. Wotton, and J. G. Hardy. Delivery of propellant soluble drug from a metered dose inhaler. *Thorax* 46:245–247 (1991).
13. J. Mortensen, S. Groth, P. Lange, and F. Hermansen. Effect of terbutaline on mucociliary clearance in asthmatic and healthy subjects after inhalation from a pressurized inhaler and a dry powder inhaler. *Thorax* 46:817–823 (1991).
14. S. P. Newman, A. W. B. Weisz, N. Talee, and S. W. Clarke. Improvement of drug delivery with a breath actuated pressurized aerosol for patients with poor inhaler technique. *Thorax* 46:712–716 (1991).
15. P. Vidgren, M. Vidgren, K. Laurikainen, T. Pietil, M. Silvasti, and P. Paronen. In vitro deposition and clinical efficacy of two sodium cromoglycate inhalation powders. *Int. J. Clin. Pharm.* 29:108–112 (1991).
16. T. B. Martonen. Aerosol therapy implications of particle deposition patterns in simulated human airways. *J. Aerosol Med.* 4:25–40 (1991).
17. M. Vidgren, M. Silvasti, P. Vidgren, K. Laurikainen, H. Lehti, and P. Paronen. Physical properties and clinical efficacy of two sodium cromoglycate inhalation aerosol preparations. *Acta Pharm. Nord.* 3:1–4 (1991).
18. M. L. Groth and W. M. Foster. Aerosolized atropine sulfate, influence of inhalation pattern on effective blockade of vagal airway tone. *Am. Rev. Resp. Dis.* 145:215–219 (1992).
19. M. Dolovich, M. Vanzieleghem, K. G. Hidinger, and M. T. Newhouse. Influence of inspiratory flow rate on the response to terbutaline sulfate inhaled via Turbuhaler^{R}. *Am. Rev. Resp. Dis.* 137:433–439 (1988).
20. S. P. Newman, F. Moren, E. Trofast, N. Talaee, and S. W. Clarke. Terbutaline sulfate Turbuhaler, effect of inhaled flow rate on drug deposition and efficacy. *Int. J. Pharm.* 74:209–213 (1991).
21. P. Malmberg, K. Larsson, and S. Thunberg. Increased lung deposition and biological effect of methacholine by the use of a drying device for bronchial provocation tests. *Eur. Resp. J.* 4:890–898 (1991).
22. J. Heyder, J. Gebhart, G. Rudolph, C. F. Schiller, and W. Stahlhofen. Deposition of particles in the human respiratory tract in the size range 0.005–15 μm. *J. Aerosol Med.* 17:811–825 (1986).
23. T. B. Martonen. Analytical model of hygroscopic particle behavior in human airways. *Bull. Math. Biol.* 44:425–442 (1982).
24. T. B. Martonen, R. C. Graham, and W. Hofmann. Human subject age and activity level, factors addressed in a biomathematical deposition program for extrapolation modeling. *Health. Phys.* 57:49–59 (1989).
25. I. Balashazy, T. B. Martonen, and W. Hofmann. Fiber deposition in airway bifurcations. *J. Aerosol Med.* 3:243–260 (1990).
26. E. Weibel. *Morphometry of the Human Lung*, Springer-Verlag, Berlin, 1963.
27. T. B. Martonen. On the fate of inhaled particles in the human, a comparison of experimental data with theoretical computations based on a symmetric and asymmetric lung. *Bull. Math. Biol.* 45:409–424 (1983).
28. J. Heyder and G. Rudolf. Deposition of aerosol particles in the human nose. In W. H. Walton (ed.), *Inhaled Particles IV*, Oxford, Pergamon Press, Oxford, 1977, pp. 107–126.
29. F. J. Miller, T. B. Martonen, M. G. Menache, R. C. Graham, D. M. Spektor, and M. Lippmann. Influence of breathing mode and activity level on the regional deposition of inhaled particles and implications for regulatory standards. In J. Dodgson, R. I. McCallum, M. R. Bailey, and D. R. Fisher (eds.), Pergamon Press, Oxford, 1988, pp. 3–10.
30. W. Stahlhofen, G. Rudolf, and A. C. James. Intercomparison of experimental region aerosol deposition data. *J. Aerosol Med.* 2:285–308 (1989).
31. T. B. Martonen and Z. Zhang. Comments on recent data for particle deposition in human nasal passages. *J. Aerosol Sci.* 23:667–674 (1992).
32. W. M. Foster. Is 24 hour lung retention an index of alveolar deposition? *J. Aerosol Med.* 1:1–10 (1988).
33. G. C. Smaldone, R. J. Perry, W. D. Bennett, M. S. Messina, J. Zwang, and J. Ilowite. Interpretation of "24 hour lung retention" in studies of mucociliary clearance. *J. Aerosol Med.* 1:11–20 (1988).